Molecular Vision 2006; 12:1185-98 <http://www.molvis.org/molvis/v12/a135/>
Received 12 June 2006 | Accepted 28 September 2006 | Published 17 October 2006

Luteinizing hormone-releasing hormone agonist and transferrin functionalizations enhance nanoparticle delivery in a novel bovine ex vivo eye model

Uday B. Kompella,[1,2] Sneha Sundaram,[1] Swita Raghava,[1] Edith R. Escobar[1]

[1]Department of Pharmaceutical Sciences and [2]Department of Ophthalmology, University of Nebraska Medical Center, Omaha, NE

Purpose: To determine whether topical ocular delivery of <100 nm nanoparticles can be enhanced by coating their exterior with peptide or protein ligands for cell surface receptors.
Methods: A novel ex vivo bovine eye model was validated for its integrity up to 60 min. Using this model, the uptake of 20 nm polystyrene nanoparticles (administered as a single 50 µl drop) before and after surface conjugation with deslorelin, a luteinizing hormone-releasing hormone (LHRH) agonist, or transferrin was determined at 5 and 60 min in individual layers of cornea and aqueous humor. Selected studies were done in the absence of corneal epithelium in the ex vivo model or using excised cornea and conjunctiva. LHRH and transferrin receptor mRNA and protein expression in corneal epithelium and conjunctiva were determined by real-time PCR and western blot, respectively.
Results: Corneal histology, ZO-1 immunostain pattern, and mannitol permeability were similar in controls and at the end of the ex vivo study. Corneal epithelial nanoparticle uptake in the absence of surface modification was 1.1-1.6% at 5 min and remained at about this level even at 60 min. Removal of the corneal epithelium resulted in about 22% particle uptake in the corneal stroma at 5 and 60 min compared to about 0.5% in the presence of epithelium, indicating the barrier nature of corneal epithelium. Deslorelin and transferrin conjugation enhanced corneal epithelial uptake of nanoparticles by 3- and 4.5 fold at 5 min and by 4.5- and 3.8 fold at 60 min, respectively. The total corneal uptake in 5 min is approximately 2.4, 9, and 16% with plain, deslorelin-functionalized, and transferrin-functionalized nanoparticles. In all groups, the nanoparticle uptake per unit tissue weight was in the order: corneal epithelium>stroma>endothelium with levels in the aqueous humor being undetectable. In excised cornea and conjunctiva studies, nanoparticle transport and uptake was elevated for both deslorelin and transferrin conjugated nanoparticles. Expression of LHRH and transferrin receptors was observed in corneal epithelium as well as conjunctiva.
Conclusions: The ex vivo bovine eye model is a useful tool in understanding disposition of nanoparticles after topical delivery. The corneal epithelium is a significant barrier for topical nanoparticle delivery to the anterior segment. Surface modification of nanoparticles by conjugating an LHRH agonist or transferrin is a useful approach to provide rapid, efficient delivery of intact nanoparticles into and/or across cornea and conjunctiva.

Despite the development of advanced drug delivery systems such as Ocusert® for sustained topical ocular drug delivery, eye drops continue to be the most popular drug delivery system for ophthalmic drugs. This is because of their ease of preparation and convenience of self-administration, and thus, patient acceptance. However, ocular drug delivery from eye drops is severely impeded by a short precorneal residence time of the drug, caused by tear flow and blinking. Fifty percent of a 25 µl drop of buffered saline is estimated to be cleared in 1.3 min in humans [1]. The small fraction of the dose that is retained in the precorneal area has to cross multiple ocular barriers beginning with the cornea and conjunctiva to reach intraocular tissues. Rapid precorneal clearance kinetics warrant the development of a delivery system that rapidly interacts with the cornea and conjunctiva and preferentially enters these tissues. To this end, we are investigating nanoparticulate systems.

Nanoparticles of various sizes based on polymers and biomaterials such as poly(lactide-co-glycolide; PLGA), poly(lactide; PLA), poly ε-caprolactone, albumin, and chitosan have been developed and tested in various cell culture and animal models [2-8] in order to improve ocular drug delivery. Nanoparticles can be employed for multiple purposes, including enhanced cellular uptake of poorly permeable drugs, reduced cellular and tissue clearance of drugs, and to sustain drug delivery. Precorneal residence as well as uptake of poorly permeable drugs by ocular epithelia can potentially be enhanced by topical delivery of drug containing nanoparticles. Indeed, following topical administration in rabbits, radiolabelled poly(hexyl-cyanoacrylate) particles could be detected in the tears, cornea, as well as conjunctiva for as long as 6 h [9]. Mucoadhesive polymer-based nanoparticles can further enhance precorneal residence time. Chitosan nanoparticles (about 385 nm) containing fluorescein have been shown to provide higher levels of fluorescein in rabbit cornea and conjunctiva as compared to chitosan plus fluorescein solution,

Correspondence to: Uday B. Kompella, Department of Pharmaceutical Sciences and Ophthalmology, University of Nebraska Medical Center, 985840 Nebraska Medical Center, Omaha, NE, 68198-5840; Phone: (402) 559-5320; FAX: (402) 559-5368; email: ukompell@unmc.edu

and constant levels of fluorescein could be detected in both cornea and conjunctiva for 24 h [10]. When tested for the delivery of cyclosporine A, it was found that cyclosporine A-loaded chitosan nanoparticles could maintain therapeutic levels of drug for 48 h [11].

Enhanced uptake is especially beneficial for macromolecules including peptides, proteins, and nucleic acid based drugs. Sustained ocular drug delivery is beneficial for the management of chronic disorders such as glaucoma, diabetic retinopathy, and age related macular degeneration. Our previous studies indicated that nanoparticles enhance the efficacy of an antisense oligonucleotide for inhibiting VEGF expression in cultured retinal pigment epithelial cells [12]. Further, these cells exhibited a remarkable ability to take up particulate systems, especially nanoparticles. Day 8 confluent human retinal pigment epithelial (ARPE 19) cell monolayers (0.75 cm^2) showed an uptake of 18% of 20 nm carboxylate fluospheres at the end of 3 h incubation of cells with the particle suspension [13]. While nanoparticle uptake by phagocytic RPE cells may be very efficient, uptake by other epithelial tissues, such as cornea and conjunctiva, is likely to be less efficient.

Although nanoparticles have been shown to increase drug levels in ocular tissues for some drugs, in this manuscript we hypothesized and demonstrated that the percentage uptake of nanoparticles relative to the initial dose is minimal in the tissues of the anterior segment. To better utilize nanomedicines, there is a need to develop nanosystems with better uptake by ocular tissues. To this end, the second objective of this manuscript was to assess the ability of surface conjugation of ligands to increase nanoparticle uptake and transport. We hypothesized that the delivery of nanoparticles can be enhanced by coating particle surface with peptide/protein ligands that enable recognition of particles by of cell surface receptors. Specifically nanoparticles functionalized with deslorelin, a nonapeptide LHRH agonist, and transferrin, a protein, have been investigated for the first time for their uptake characteristics into various layers of bovine cornea, i.e., epithelium, stroma, and endothelium as well as aqueous humor using an ex vivo bovine eye model. In addition, select transport studies were conducted with excised cornea and conjunctiva.

METHODS

Materials: Polystyrene fluospheres®, 20 nm in diameter, surface modified with carboxylate functionalities, were purchased from Molecular Probes (Carlsbad, CA). Deslorelin was a gift from Balance Pharmaceuticals, Inc. (Santa Monica, CA). Transferrin, propidium iodide and the chemicals required for making buffer solutions were purchased from Sigma-Aldrich (St. Louis, MO). ^{3}H-mannitol was obtained from American Radiolabeled Chemicals, Inc. (St. Louis, MO). Rabbit anti-ZO1 antibody was obtained from Zymed (Carlsbad, CA). Alexa 488 secondary antibody was obtained from Molecular Probes.

Buffers: Uptake using the ex vivo model and transport experiments using excised tissues were carried out by preparing particle suspensions in assay buffer (pH 7.4), containing 1.14 mM $CaCl_2$, 1.2 mM $MgSO_4$, 3 mM KCl, 0.4 mM KH_2PO_4, 25 mM $NaHCO_3$, 10 mM glucose, 122 mM NaCl, and 10 mM HEPES (N-2-hydroxyethylpiperazine-N'-2-ethanesulphonic acid) [14]. Assay buffer was pre-equilibrated to 37 °C or 4 °C for 30 min prior to each experiment. The assay buffer, adjusted to pH 5.0 (acid buffer) with HCl, was used as a wash solution to remove any tissue adherent nanoparticles.

Preparation of peptide/protein conjugated nanoparticles: Nanoparticles (NP) conjugated to deslorelin (deslorelin-NP) or transferrin (transferrin-NP) were prepared by covalent conjugation of the protein to the carboxylate surface functionality on the nanoparticles using carbodiimide. Briefly, 5 ml of 2 mg/ml NP suspension in 3(N-Morpholino) propanesulfonic acid (MOPS) buffer was added dropwise to 5 ml of 200 µg/ml protein solution. The mixture was allowed to react at room temperature for 15 min. Carbodiimide (4 mg) was added to the reaction mixture and the pH adjusted to 7.3-7.4. The reaction mixture was allowed to incubate at room temperature for 2 h with vortexing. After 2 h, the reaction was quenched by the addition of 100 mM glycine. The conjugated particles were separated from unreacted protein by dialyzing across a membrane having a 50,000 molecular weight cut off (Spectra/Por, Spectrum Laboratories, CA).

Nanoparticle characterization: The particle size and the zeta-potential were measured using a Zeta Plus zeta-potential analyzer, Brookhaven Instruments Ltd. (New York, NY), which employs a dynamic light scattering technique for particle size measurement. The particle size and zeta-potential measurements were made after 1:1000 dilution of particle stock in filtered deionized water. Further, the particles were visualized using a transmission electron microscope (TEM). Briefly, the carbon-coated grids were floated on a suspension droplet of plain or functionalized nanoparticles on a flexible plastic film (Parafilm, Pechiney Plastic Packaging, Neenah, WI) to allow the adsorption of nanoparticles onto the grid. After drying the particles, uranyl acetate was added as a negative stain to the carbon grid and allowed to react with the particles. This procedure makes the particles electron dense, allowing their visualization using an electron microscope. The particles were photographed using a EM410 Phillips electron microscope (Eindhoven, The Netherlands) set at 60 kV and a magnification of 153,000X.

Excised bovine eye model for eye drop studies: Freshly excised bovine eyes were obtained from a local slaughter house (Nebraska Beef, Omaha, NE). The experiments were initiated within 2-3 h after sacrifice. For the experiment, bovine eyes were placed in Teflon coated wells containing assay buffer to immerse the posterior segment while exposing the cornea towards the surface. The Teflon coated well plate was placed in a shaking water bath maintained at 37 °C and the water bath was sealed with Saran Wrap™ (S.C. Johnson & Son, Inc., Racine, WI). Alternatively, the setup was placed in a cold room maintained at 4 °C. Prior to dosing, the eyes were equilibrated for about 30 min with assay buffer at 37 °C or 4 °C as required. The measured temperatures of the vitreous humor and aqueous humor in the 37 °C study were about 37 °C and 35

°C, respectively. The measured temperature was about 5 °C for both vitreous humor as well as aqueous humor in the 4 °C study. In the ex vivo studies, either 5 or 60 min time points were chosen since eye drops are rapidly cleared from the tissue surface and because high solute uptake is desired in a short time with eye drops.

Ex vivo model studies involved administration of a 50 µl dosing solution/suspension drop to the cornea followed by 50 µl drops of assay buffer on the cornea every 15 min to maintain corneal moisture. At the end of 0, 5, or 60 min, the corneal surface was washed thrice with assay buffer (1 ml each time) followed by three washes with acid buffer (1 ml each time) to remove any loosely adherent nanoparticles prior to tissue analysis. The same protocol was followed even when plain buffer drops were assessed.

Immunohistochemistry for ZO-1: To assess the tight junctional architecture in the ex vivo bovine eye model for the duration of the uptake studies, corneas isolated at the beginning and end of the experiment were labeled with anti-ZO1 antibody. For the experiment, a 50 µl drop of assay buffer was topically administered to isolated bovine eyeballs. The cornea was kept moist for the duration of the experiment by instilling 50 µl drops of assay buffer on the cornea every 15 min. At 5 and 60 min after first drop instillation, the eyes were washed thrice with 1 ml assay buffer followed by three washes (1 ml each time) with acid buffer, and the corneas were excised and fixed in 2% paraformaldehyde for 15 min at room temperature. The tissues were then permeabilized for 30 min at room temperature with 0.1% Triton-X solution in PBS containing 5% goat serum. The tissues were subsequently incubated with rabbit anti-ZO1 primary antibody (1:100) for 1 h. The tissues were washed thrice with PBS for 15 min. Subsequently tissues were incubated for 1 h with Alexa 488 secondary antibody (1:500). The tissues were again washed thrice with PBS and were finally stained with 1 µg/ml propidium iodide for 5 min. The stained tissues were then imaged using a confocal microscope at 63X magnification.

Tissue histology: For histology, at 0 (control), 5, and 60 min after instillation of 50 µl assay buffer drop and buffer treatments as described above, corneas were isolated and immediately transferred to a 10% neutral buffered formalin solution. The tissues were subsequently embedded in paraffin and 4 µm thick sections were cut. The sections were stained with hematoxylin and eosin and viewed with a Zeiss Axioscope 40 microscope. Images were taken with a Hitachi HV-D25 digital camera using EPIX-XCAPLite software V2.2 for windows.

Integrity of corneal barrier in the ex vivo model with or without nanoparticle exposure: ^{3}H-Mannitol transport across the excised bovine cornea was performed without any treatment or after dosing the bovine ex vivo eye model with a 50 µl drop of assay buffer or 50 µl of 1 mg/ml nanoparticle suspension, followed by incubation up to 60 min with buffer treatments, as described above. At 5 and 60 min after assay buffer drop instillation and 60 min after nanoparticles drop instillation, the eyes were washed thrice with assay buffer (1 ml each time) and the corneas were isolated from the eyeball. The tissues were then mounted in modified Ussing chambers (Navicyte, Reno, NY) for the mannitol transport study. The aperture area of the chambers was 0.64 cm^2. The corneal area exposed is expected to be slightly greater than the chamber aperture area due to corneal curvature. ^{3}H-mannitol (1.5 ml; 1 µCi/ml) was placed in the donor chamber (epithelial to endothelial transport) and plain assay buffer (1.5 ml) was placed in the receiver chamber. At various time points (up to 4 h), 200 µl samples were removed from the receiver chamber and replaced with an equal volume of fresh assay buffer. To each sample, 4 ml of scintillation fluid (Fisher Scientific, NJ) was added and the radioactivity was quantified using a liquid scintillation counter.

Nanoparticle uptake studies using the ex vivo bovine eye model: To initiate the experiment, a 50 µl eye drop of 10 mg/ml (in studies assessing the influence of epithelium in particle uptake) or 1 mg/ml nanoparticle suspension was topically administered to isolated bovine eyeballs. Buffer and wash treatments were performed as described above. At 5 and 60 min after drop instillation, the incubation was terminated and the corneal epithelium, stroma, endothelium, and aqueous humor (0.5 ml) were removed from the eyeball. The tissues were homogenized in 2% Triton-X. The supernatant obtained after centrifuging tissue homogenate at 5,000 rpm (Marathon Micro AR, Fisher Scientific) for 10 min was analyzed by spectrofluorometry at excitation and emission wavelengths of 505 and 515 nm, respectively.

Nanoparticle uptake and transport studies using excised bovine cornea and conjunctiva mounted in vertical diffusion chambers: The above described modified Ussing chambers were used to mount bovine corneas and conjunctivas for nanoparticle transport studies. The tissues were exposed to 1.5 ml of assay buffer with either conjugated or unconjugated nanoparticles (100 µg/ml) on the mucosal/tear side (donor side). The receiver side was exposed to 1.5 ml of assay buffer without nanoparticles. The buffers were pre-equilibrated to 37 °C or 4 °C as required and the chambers were maintained at the desired temperature. Samples were collected from the receiver chamber at various intervals up to 4 h and the receiver chamber was replenished with an equal volume of temperature pre-equilibrated assay buffer. The experiment was terminated at 4 h and the samples were stored in polypropylene tubes at 4 °C until analysis.

At the end of the 4 h transport studies, the tissue area exposed to particle suspension were cut and washed thrice with assay buffer followed by the acid buffer (pH 5.0). The tissues were then homogenized in 2% Triton-X using Tissue Tearor™. The tissue debris was separated by centrifugation at 3,000 rpm (Marathon Micro AR) for 10 min. The supernatant was collected to analyze the amount of nanoparticles taken up by the tissue. The supernatant was analyzed by spectrofluorometry at excitation and emission wavelengths of 505 and 515 nm, respectively.

Confocal microscopy to determine nanoparticle uptake in different layers of cornea and conjunctiva: The transport

procedure described above for excised tissues was followed. At the end of 4 h, the tissue exposed to the particles suspension was isolated and frozen in a tissue freeze solution, and 4 μm thick sections were cut. The tissue sections were then imaged using a confocal microscope at 20X magnification to determine nanoparticle uptake in the various regions of cornea (epithelium, stroma, and endothelium) and conjunctiva (epithelium and stroma).

Real-time PCR for receptor mRNA expression: The expression of LHRH receptor (LHRH-R), transferrin receptor 1 (TfR1), and transferrin receptor 2 (TfR2) mRNA levels were quantified relative to the expression of these receptors in the pituitary by real time polymerase chain reaction (real-time PCR). RNA isolation from bovine conjunctiva and corneal epithelium was carried out using the RNA STAT-60 RNA isolation kit (Tel-Test, Friendswood, TX). Briefly, freshly excised tissues (pituitary, corneal epithelium, and conjunctiva) were homogenized in 1 ml RNA STAT-60 (Tel-Test, Friendswood, TX) solution, followed by extraction with 200 μl of chloroform. The tissue debris, DNA as well as proteins, were separated into the organic phase by centrifugation at 12,000 g for 15 min at 4 °C. The aqueous phase contained RNA. Further extraction was carried out with isopropanol (1:1 v/v ratio with the aqueous phase). RNA was precipitated and separated by centrifugation at 12,000 g for 15 min at 4 °C. The RNA pellet obtained was washed with 70% ethanol. Purified RNA was separated by centrifugation at 7,500 g for 5 min at 4 °C. The pellet was air dried and redissolved in 100 μl of nuclease free water by incubation at 55 °C for 15 min. Care was taken to not over dry the pellet in order to facilitate redissolution. The RNA samples were analyzed with UV spectrophotometry. Samples with an A_{260} to A_{280} ratio equal to or more than 1.8 were considered to be free of DNA and protein contamination.

RNA (5 μg) isolated from bovine corneal epithelium and conjunctiva was converted into cDNA by reverse transcription. Real-time PCR was carried out using the ABI PRISM 7500 Sequence Detection System (Applied Biosystems). The reactions were performed with 2X SYBR Green PCR master mix (Applied Biosystems), in the presence of 30 ng cDNA and 300 nM of specific primer sets. Samples were analyzed in triplicate. Amounts of input RNAs in each sample were corrected for by dividing threshold cycle (Ct) of each specific gene by the Ct for 18s rRNA. Fold values were calculated as $2^{-\Delta Ct}$, where ΔCt=Ct for the specific gene minus Ct for 18s rRNA in the same RNA. The sample with the lowest expression was set to 1.0 fold and other data were adjusted to that baseline [15,16]. The primers used for LHRH receptor type 1 (for the LHRH-R, based on blast analysis of the sequence of the primer, the receptor subtype was identified as LHRH-R type 1) were; sense 5'-GAC CTT GTC TGG GAA AGA TCC-3' and antisense 5'-CAG GCT GAT CAC CAC CAT CA-3'; for the transferrin receptor 1 (TfR1), sense 5'-AGG AAC CGA GTC TCC AGT GA-3' and antisense 5'-ATC AAC TAT GAT CAC CGA GT-3' [17]; for the transferrin receptor 2 (TfR2), sense 5'-GTG GTC AGT TGA GGA TGT CAA-3' and antisense 5'-CCA CAC GTG GTC CAG CTT CTG GCG GGA G-3' [18]; and for 18S rRNA, sense 5'-GAT ATG GCT CAT GTG GTG TTG-3' and antisense, 5'-AAT CTT CTT CAG TCG CTC CA-3'.

Western blots for LHRH and transferrin receptors: Homogenates of freshly excised tissues (pituitary, corneal epithelium, and conjunctiva) were prepared as follows. About 200 mg of tissue was homogenized using a Tissue Tearor™ in tissue protein extraction reagent (T-PER, Pierce, Rockford, IL). After homogenization, the suspension was centrifuged at 3,000 rpm at 4 °C to separate the tissue debris. The supernatant was aliquoted and stored at -80 °C until further use. Total protein content of each tissue homogenate was estimated using the Pierce BCA kit (Pierce Biotechnology, Inc., Rockford, IL). Tissue samples (20 μg of protein) were then loaded onto polyacrylamide gels. Molecular weight markers ranging from 14.3 to 220 kDa (Amersham Life Science, Arlington Heights, IL) were used to identify LHRH receptor, transferrin receptors, and α-actin protein bands. The proteins were separated using preformed 10% polyacrylamide gels (Bio-Rad, Hercules, CA) and sodium dodecyl dulfate-polyacrylamide gel electrophoresis (SDS-PAGE). The gels were run at 60 V for 10 min and then continued at 120 V for another 1.5 h. The proteins were then transferred to polyvinylidene fluoride (PVDF) membranes (Millipore, Bedford, MA) at 4 °C using a current of 480 mA. Immunoblotting was performed with specific antibodies for LHRH receptor (1:100 dilution; LabVision, Freemont, CA), transferrin receptor-1 (1:1,000 dilution; Biodesign International, Saco, ME), and transferrin receptor-2 (1:1,000 dilution; Abcam Inc, Cambridge, MA) or the monoclonal anti α-actin antibody (1:1,000 dilution; Sigma-Aldrich, St Louis, MO) after treatment with blocking buffer containing 0.3% Tween, 1% BSA, and 5% non-fat dry milk. Incubation with antibody was done overnight at 4 °C. Following washes with Tris buffer at pH 7.4, secondary antibody, horseradish peroxidase conjugated mouse or rabbit immunoglobulin (IgG; Jackson Immunoresearch, West Grove, PA), was added (1:1,500) as needed and incubated at 4 °C for 1 h. Protein bands were visualized using a ECL-Plus chemiluminescence kit (Amersham Biosciences, Piscataway, NJ).

Statistical analysis: Data is expressed as mean±SD. Comparison of means of various groups was done using nonparametric statistical analysis. Comparison of two groups was carried out using Mann Whitney test, however for comparison of

Table 1.

Particle type	Measured diameter (nm)	Polydispersity	Zeta potential (mV)
NP	85.2±0.6	0.282±0.004	−57.93±4.55
Deslorelin-NP	98.2±0.6	0.223±0.021	−35.76±1.73
Transferrin-NP	84.7±0.8	0.224±0.010	−29.24±4.33

Physical properties of various nanoparticles used. The data are expressed as mean±SD for n=3. NP; polystyrene nanoparticles with carboxylate surface functional group, Deslorelin-NP; deslorelin conjugated carboxylate nanoparticles, and Transferrin-NP; transferrin conjugated carboxylate nanoparticles.

more than two groups, Kruskal Wallis nonparametric ANOVA was employed. Differences were considered statistically significant at p less than or equal to 0.05.

RESULTS

Physicochemical characteristics of nanoparticles: The effective diameter, polydispersity index, and zeta-potential of NP, deslorelin-NP, and transferrin-NP are summarized in Table 1. The diameters shown include a hydrodynamic layer around particles and the actual physical diameter is expected to be smaller, as evidenced in the transmission electron micrographs (Figure 1). In TEM images, deslorelin-NP and transferrin-NP exhibited somewhat darker surfaces compared to unconjugated nanoparticles. This is consistent with the uptake of electron

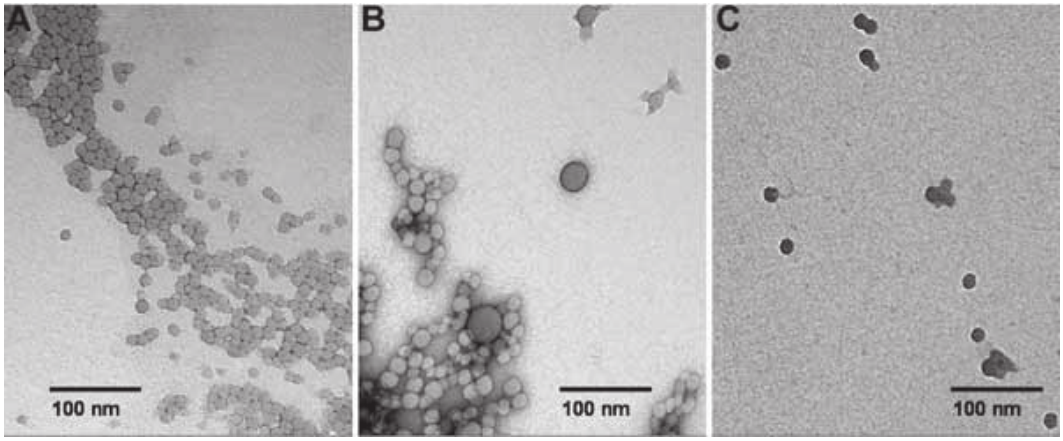

Figure 1. Transmission electron microscopy of nanoparticles. **A**, **B**, and **C** represent TEM pictures of NP, deslorelin-NP, and transferrin-NP, respectively. The TEM pictures were obtained at a magnification of 153,000X.

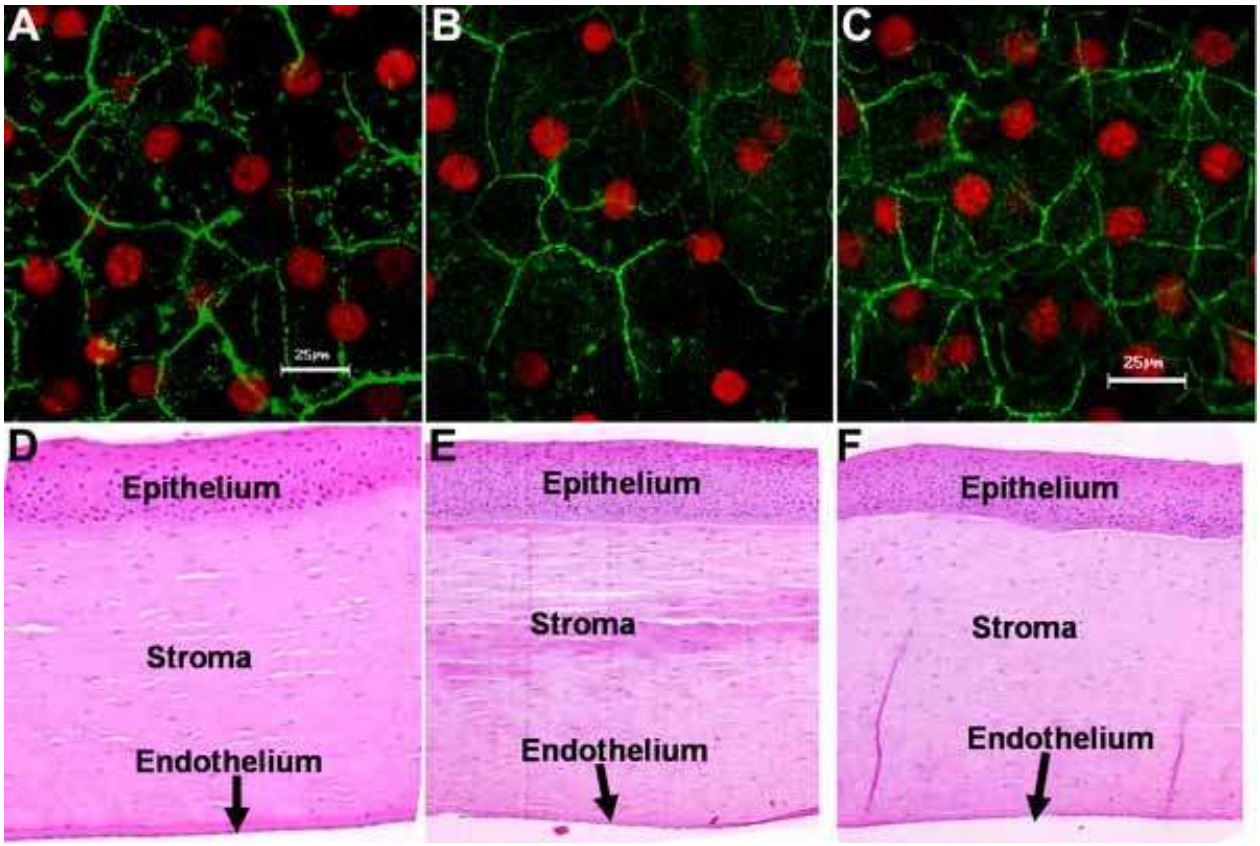

Figure 2. Corneal epithelial tight junctional architecture and histology in a bovine ex vivo eye model treated with plain buffer. **A**, **B**, and **C** represent confocal images of bovine corneas double labeled with anti-ZO1 antibody (green) and propidium iodide (red) at 0 (control), 5, and 60 min, respectively, in the ex vivo study with plain buffer treatment at 37 °C. **D**, **E**, and **F** show representative histology pictures (magnification 5X) of cornea after hematoxylin and eosin staining at 0 (control), 5, and 60 min, respectively, in the ex vivo study with plain buffer. The confocal images were obtained at a magnification of 63X.

microscopy stain by peptide/protein ligands on particle surfaces.

Corneal integrity is preserved in the ex vivo bovine eye model and the nanoparticle formulations do not alter corneal integrity: The barrier properties of the cornea remain unaffected for at least 60 min in the ex vivo bovine model (Figure 2A-C). No significant differences were seen in the ZO1 staining pattern in freshly excised cornea and corneas following incubation for 5 or 60 min. Further, no differences were observed in the histology of these preparations (Figure 2D-F). The corneal ZO1 staining patterns in the presence of NP, deslorelin-NP, and transferrin-NP were also similar to controls instilled with similar volume of assay buffer (Figure 3). Further, the apparent permeability coefficient of mannitol, a paracellular marker, did not differ significantly between freshly isolated corneas ($0.4\pm0.1x10^{-6}$ cm/s) and the corneas isolated at 5 ($0.5\pm0.1x10^{-6}$ cm/s) and 60 min ($0.47\pm0.04x10^{-6}$ cm/s) following exposure to 50 µl assay buffer drop in the ex vivo study (Figure 4A). Additionally, mannitol permeability did not differ between NP ($0.41\pm0.18x10^{-6}$) and deslorelin-NP ($0.41\pm0.04x10^{-6}$) or transferrin-NP ($0.37\pm0.08x10^{-6}$ cm/s) groups or between nanoparticle groups and assay buffer treated group when permeability was assessed across corneas isolated at 60 min following exposure to 50 µl of various formulations in assay buffer (Figure 4B).

Nanoparticle uptake is significantly hindered by corneal epithelium in the ex vivo eye model: The concentration of nanoparticles in various layers of cornea, at 5 and 60 min after topical instillation, of a 50 µl drop of 10 mg/ml carboxylate nanoparticle suspension to isolated bovine whole eyeball followed the order: epithelium>stroma>endothelium. The concentration of nanoparticles detected after 5 (Figure 5C) and 60 min (Figure 5E) in bovine corneal epithelium was 255.76±123.6 and 208.7±67 ng/mg tissue/mg dose and in corneal stroma it was 8.85±18 and 12.2±21 ng/mg tissue/mg dose, respectively. However, no nanoparticles were detected in the endothelium or aqueous humor at the two time points.

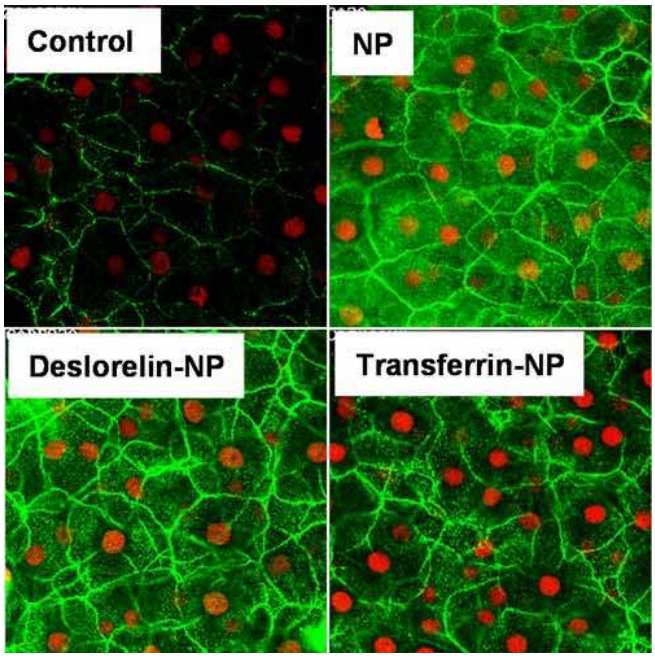

Figure 3. Corneal epithelial tight junctional architecture is retained in the bovine ex vivo eye model treated with nanoparticles. Panels represent control ZO1 staining pattern and nuclear staining in control (untreated), NP, deslorelin-NP, and transferrin-NP treated bovine cornea in ex vivo model at the end of 60 min study at 37 °C. The confocal images were obtained at a magnification of 63X.

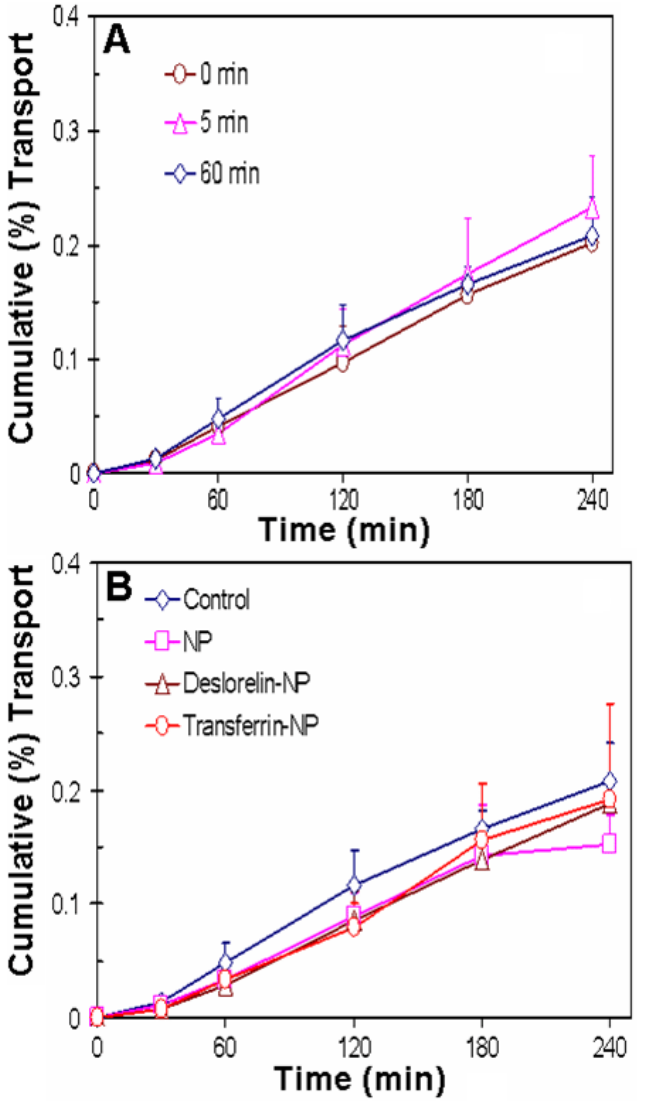

Figure 4. Corneas retain barrier integrity during the ex vivo bovine eye study with or without nanoparticle treatment. A 50 µl drop of either assay buffer (control) or 1 mg/ml nanoparticle suspension was topically instilled in the ex vivo bovine eye model maintained at 37 °C. After 0, 5, and 60 min of exposure to assay buffer and 60 min exposure to nanoparticle suspensions, corneas were isolated and permeability of ^{3}H-mannitol, a paracellular marker, was assessed. Percent cumulative transport is plotted for corneas obtained after assay buffer drop administration and ex vivo study termination at various time points (**A**) or after nanoparticle suspension administration followed by ex vivo study termination at 60 min (**B**). The data are expressed as mean±SD for n=4.

The removal of corneal epithelium, as confirmed by tissue histology using H&E staining (Figure 5A,B) prior to topical nanoparticle suspension administration, increased particle uptake at 5 and 60 min in corneal stroma by 45- and 32 fold, respectively. The concentration of nanoparticles detected after 5 (Figure 5D) and 60 min (Figure 5F) in bovine corneal stroma was 402.6±113 and 385.02±136 ng/mg tissue/mg dose, respectively, and in the endothelium it was 45.67±29.7 and 166.75±204 ng/mg tissue/mg dose, respectively. However, no nanoparticles could be detected up to 60 min in the aqueous humor even in the absence of corneal epithelium.

The percent nanoparticle dose delivered with and without the epithelium is summarized in Table 2. The total tissue amounts were arrived at by multiplying tissue concentrations with the average weights indicated in Table 2 for each tissue in its entirety.

Nanoparticles functionalized with deslorelin and transferrin exhibit better uptake in the ex vivo eye model: Compared to unconjugated nanoparticles, deslorelin- and transferrin-conjugated nanoparticles had significantly higher uptake into the corneal epithelium of the ex vivo bovine eye model following topical instillation of 50 µl of 1 mg/ml particle suspension. The uptake of NP, deslorelin-NP, and transferrin-NP by corneal epithelium at 5 min after eyedrop instillation was 169±28, 539±225, and 791±239 ng/mg tissue/mg dose, respectively (Figure 6A). At 60 min, the corresponding values were 304±120, 1362±612, and 1146±307 ng/mg tissue/mg dose, respectively (Figure 6B). Thus, corneal epithelial uptake in 5 min for deslorelin-NP and transferrin-NP was 3 fold and 4.5 fold higher than unconjugated nanoparticles. At 60 min, the uptake was 4.5- and 3.8 fold higher with deslorelin-NP and transferrin-NP, respectively. The nanoparticle delivery expressed as percent dose delivered is summarized in Table 3 for NP, deslorelin-NP, and transferrin-NP.

Corneal epithelial uptake of deslorelin-NP and transferrin-NP was also assessed in the presence of free conjugating ligand and at low temperature (4 °C). The uptake of these particles was significantly decreased in the presence of free deslorelin (1 mg/ml) and transferrin (1 mg/ml), respectively (Table 4), and at 4 °C, indicating the involvement of a receptor mediated process.

Nanoparticle functionalization enhances transport and uptake in excised bovine cornea and conjunctiva: Conjugation of deslorelin and transferrin to nanoparticle surfaces significantly enhanced the transport of nanoparticles across bovine cornea and conjunctiva. The cumulative transport of NP, deslorelin-NP, and transferrin-NP in 4 h across isolated bo-

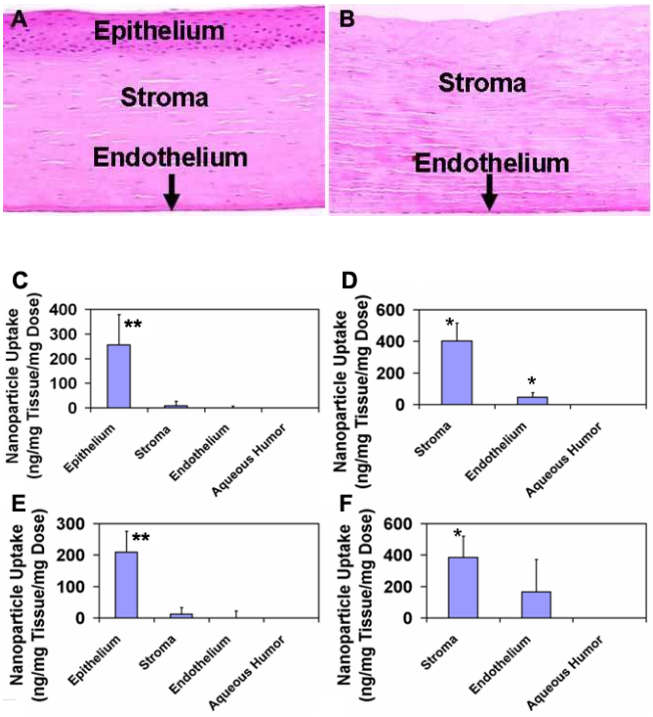

Figure 5. Corneal epithelium is a substantial barrier for nanoparticle delivery in the bovine ex vivo eye model. After instillation of a 50 µl drop of 10 mg/ml plain nanoparticles and 5 or 60 min uptake study at 37 °C, the tissue layers were isolated, homogenized, and particle uptake was quantified. The figure shows bovine cornea with (**A**) and without epithelium (**B**) and uptake of nanoparticles at 5 min (**C**, **D**) and 60 min (**E**, **F**) in intact bovine eyes (**C**, **E**) or those devoid of corneal epithelium (**D**, **F**). The data are expressed as mean±SD for n=3. Magnification in **A** and **B** was 5X. The asterisk indicates a $p<0.05$ compared to the group on the left with epithelium. The double asterisk indicates a $p<0.05$ compared to stroma, endothelium, and aqueous humor.

Table 2.

Corneal layer	Tissue weight (g) (with epithelium)	Tissue weight (g) (without epithelium)	NP uptake at 5 min (%) With epithelium	NP uptake at 5 min (%) Without epithelium	NP uptake at 60 min (%) With epithelium	NP uptake at 60 min (%) Without epithelium
Epithelium	0.0627±0.002	–	1.60	–	1.31	–
Stroma	0.5139±0.021	0.5601±0.038	0.45	22.54	0.63	21.56
Endothelium	0.0083±0.001	0.0086±0.001	ND	0.039	ND	0.143

Nanoparticle uptake into various layers of bovine cornea in the bovine ex vivo model. The data are expressed as mean±SD for n=3. ND; Not detectable. Tissue weights with epithelium were measured at time zero and those without epithelium were measured at the end of 60 min incubation. Note that there are no significant differences in the weights of stroma and endothelium between the two groups. A dosing solution of 10 mg/ml nanoparticles at 50 µl volume was used. All other studies employed 1 mg/ml concentration.

vine cornea at 37 °C was 0.65±0.01, 1.85±0.09, and 2.76±0.03%, respectively (Figure 7). The corresponding values for conjunctiva were 1.8±0.09, 3±0.09, and 3.5±0.1%, respectively. Thus, conjugation of deslorelin and transferrin to the surface of nanoparticles increased the percent transport of nanoparticles across bovine cornea by 64 and 74%, respectively. The corresponding increase for conjunctiva was 40 and 51%, respectively. Interestingly, the nanoparticles were below detection limits in the receiver chamber up to 180 min for cornea and up to 120 min for conjunctiva, suggesting a significant lag time for the transport of nanoparticles.

When the transport study was conducted at 4 °C, corneal transport of all nanoparticles was completely abolished, with no detectable amounts of nanoparticles in the receiver chamber even at 4 h. In conjunctiva, on the other hand, the reduc-

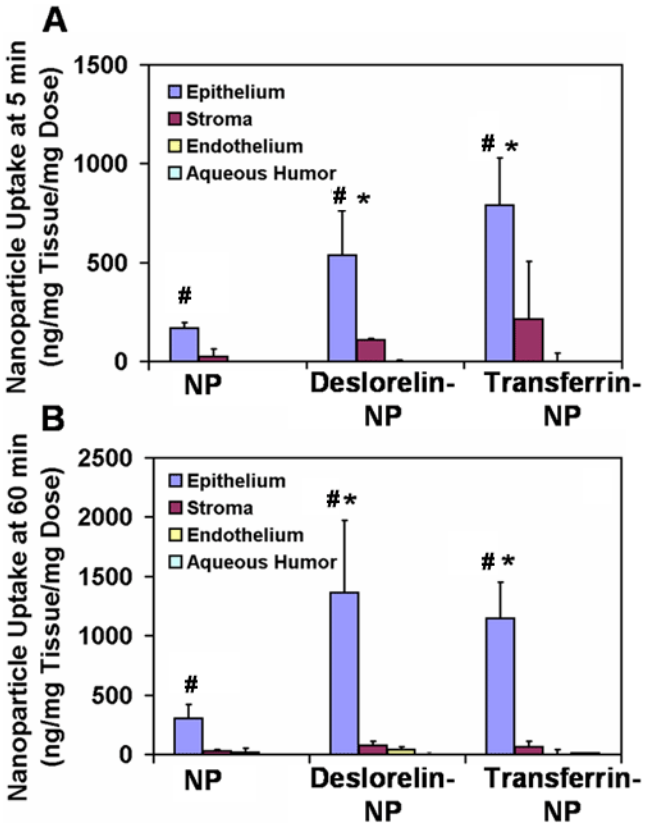

Figure 6. Deslorelin and transferrin functionalizations enhance corneal nanoparticle uptake in the bovine ex vivo eye model. A 50 µl drop of 1 mg/ml nanoparticle suspension (NP, deslorelin-NP, and transferrin-NP) was topically instilled on an isolated bovine eye maintained at 37 °C. After 5 (**A**) and 60 min (**B**), particle uptake in corneal epithelium, stroma, endothelium, and aqueous humor was quantified. The data are expressed as mean±SD for n=3. The asterisk indicates a p<0.05 compared to NP group and the sharp (hash mark) indicates a p<0.05 compared to stroma, endothelium, or aqueous humor.

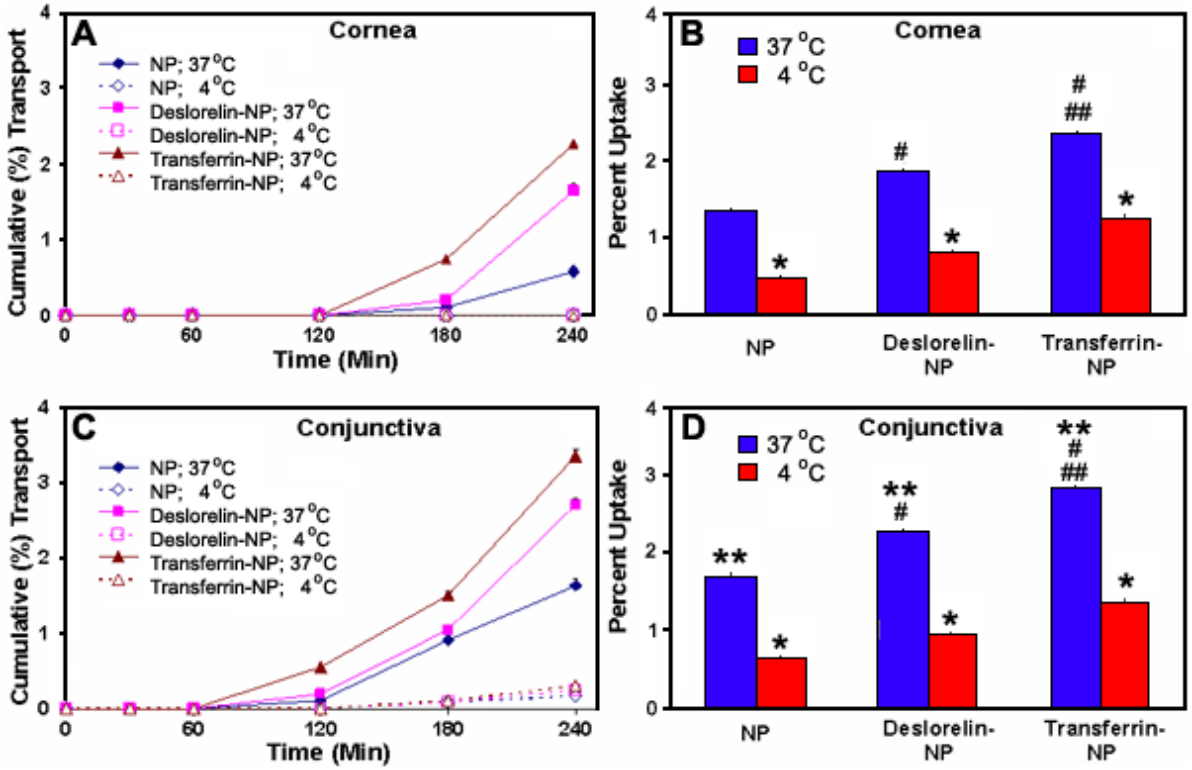

Figure 7. Deslorelin and transferrin functionalizations enhance nanoparticle transport (**A**, **C**) and uptake (**B**, **D**) in isolated corneas and conjunctivas determined using an Ussing chamber setup. Nanoparticles (NP, deslorelin-NP and transferrin-NP) were exposed to isolated bovine cornea and conjunctiva mounted in Ussing chambers. Cumulative transport or uptake at 4 h is presented. Experiments were conducted at 37 °C as well as 4 °C. The data are expressed as mean±SD for n=4. The asterisk indicates a p<0.05 compared to corresponding particles at 37 °C, the sharp (hash mark) indicates a p<0.05 compared to NP group at 37 °C, the double sharp indicates a p<0.05 compared to deslorelin-NP at 37 °C, and the double asterisk indicates a p<0.05 compared to corresponding data for corneal uptake.

tion in the cumulative transport was 87, 88, and 89%, respectively, for NP, deslorelin-NP, and transferrin-NP.

Conjugation of deslorelin and transferrin to the nanoparticle surface significantly enhanced the uptake of nanoparticles by isolated bovine conjunctiva and cornea. The uptake of NP, deslorelin-NP, and transferrin-NP by isolated bovine cornea at 37 °C was 1.35±0.03, 1.83±0.03, and 2.36±0.03%, respectively, at the end of 4 h. The corresponding uptake in bovine conjunctiva was 1.71±0.05, 2.27±0.02, and 2.83±0.03%, respectively (Figure 7C,D). At 4 °C, nanoparticle uptake was reduced significantly. The reduction in corneal uptake was 66, 56, and 47%, respectively for NP, deslorelin-NP, and transferrin-NP, respectively. The corresponding reduction in conjunctival uptake was 63, 59, and 52%, respectively (Figure 7C,D).

Confocal study of nanoparticle uptake in the various layers of the cornea and conjunctiva: To determine the uptake of nanoparticles in different layers of bovine cornea and conjunctiva, tissues exposed to nanoparticles for 4 h during transport study were isolated. They were then frozen in tissue freeze solution and sectioned to a thickness of 4 µm. The sections were visualized under a confocal laser scanning microscope at 20X magnification. Control cornea and conjunctiva were not exposed to nanoparticles. Both tissues exhibited some background auto-fluorescence. In all particle groups, the fluorescence intensities were greater than those in the controls. The fluorescent intensities of nanoparticles in various layers of the cornea, followed the order: epithelium>stroma>endothelium (Figure 8). In conjunctiva, fluorescence intensities followed the order: epithelium>stroma for transferrin-NP (Figure 9). For the other nanoparticles, the regions were less distinguishable in conjunctiva, possibly due to tissue folding upon isolation. However, nanoparticle distribution appeared less restricted in the conjunctiva compared to the cornea. The intensities of the different particles in the cornea and conjunctiva were generally in the order: transferrin-NP>deslorelin-NP>NP.

LHRH receptor and transferrin receptor mRNA and protein expression in bovine corneal epithelium and conjunctiva: Real time PCR results showed quantifiable levels of LHRH-R, TfR1, and TfR2 mRNA in both bovine corneal epithelium and conjunctiva. The LHRH-R, TfR1, and TfR2 mRNA levels in bovine corneal epithelium were 36-, 25-, and 100 fold

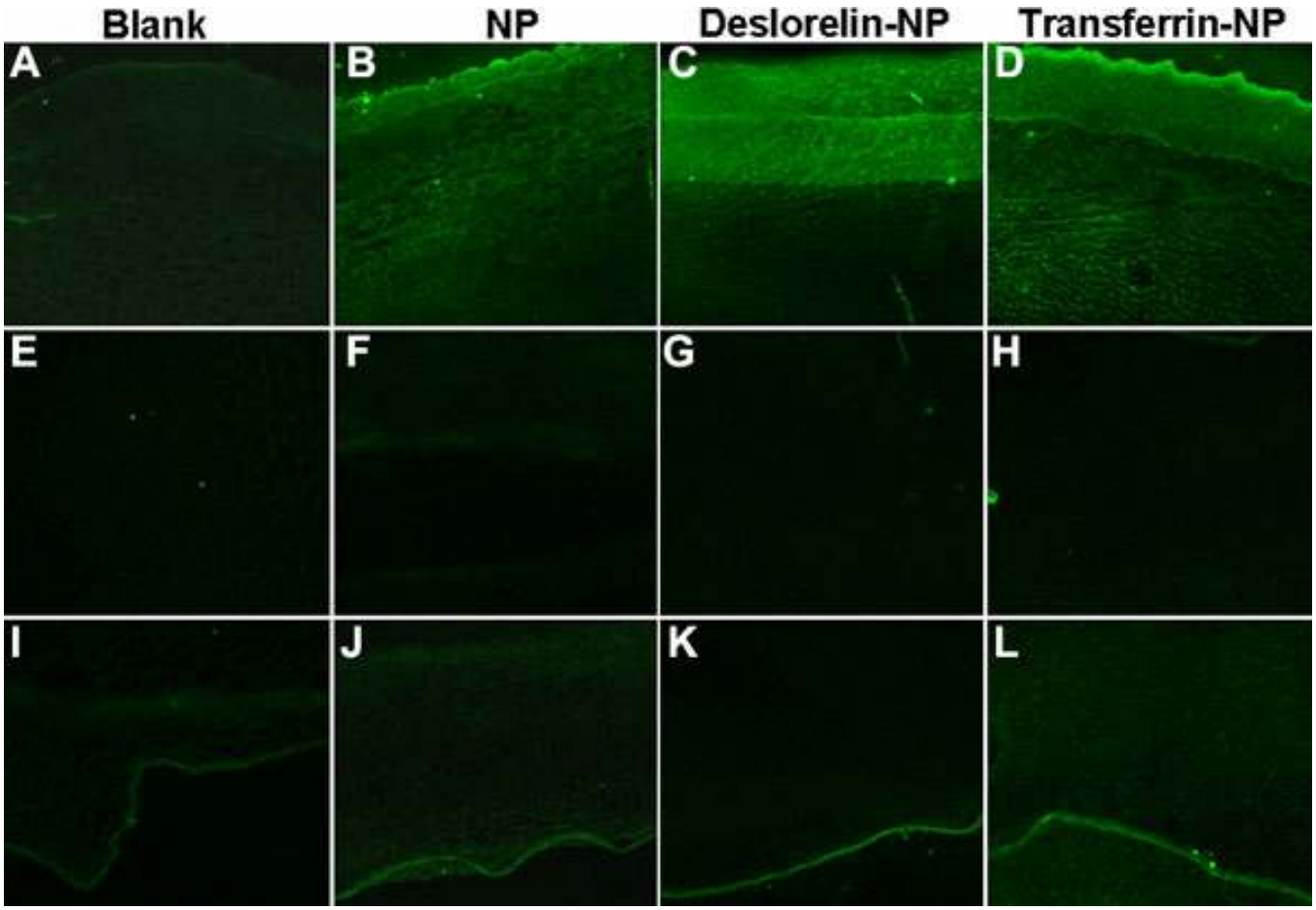

Figure 8. Representative confocal micrographs to show the uptake of nanoparticles in the epithelial, stromal, and endothelial layers of bovine cornea at the end of 4 h transport study at 37 °C using a modified Ussing chamber setup. **A**, **E**, and **I** represent the top, middle, and lower regions of blank corneal tissue without any nanoparticle exposure. Corresponding regions for NP (**B**, **F**, and **J**), deslorelin-NP (**C**, **G**, and **K**), and transferrin-NP (**D**, **H**, and **L**) are shown in various panels. The confocal images were obtained at a magnification of 20X.

lower than respective levels in the pituitary. In bovine conjunctiva LHRH-R, TfR1, and TfR2 mRNA levels were found to be 20-, 5-, and 25 fold lower than the respective levels in the pituitary (Figure 10).

Western blot showed the presence of LHRH-R protein in corneal epithelium and conjunctiva. TfR1 protein was clearly detectable in conjunctiva, but a faint band was observed in the corneal epithelium. However TfR2 was not detected in any of the tissues (Figure 11).

DISCUSSION

We have previously shown that nanoparticles can be employed to enhance retinal pigment epithelial uptake of a VEGF antisense oligonucleotide by 4 fold, resulting in efficacy comparable to lipofectamine treatment [12]. In addition, we have shown that a single periocular injection of a corticosteroid (budesonide) encapsulating poly lactic acid (PLA) nanoparticles as compared to budesonide solution results in 27-, 9-, and 5 fold higher drug levels in cornea, retina, and vitreous, respectively, at the end of day 7 in a rat model, suggesting the suitability of nanoparticles to sustain drug deliv-

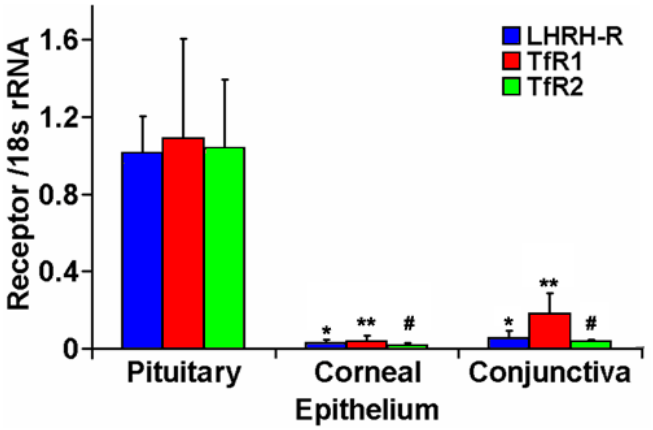

Figure 10. Differential expression of LHRH and transferrin receptors on various bovine ocular tissues. The fold difference ($2^{-\Delta Ct}$) of LHRH receptor (blue bars), transferrin receptor 1 (red bars) and transferrin receptor 2 (green bars) between the corneal epithelium and conjunctiva is presented as mean±SD for n=3 samples. The asterisk indicates a $p<0.05$ compared with LHRH-R, the double asterisk indicates a $p<0.05$ compared with TfR1, and the sharp (hash mark) indicates a $p<0.05$ compared with TfR2, in the pituitary.

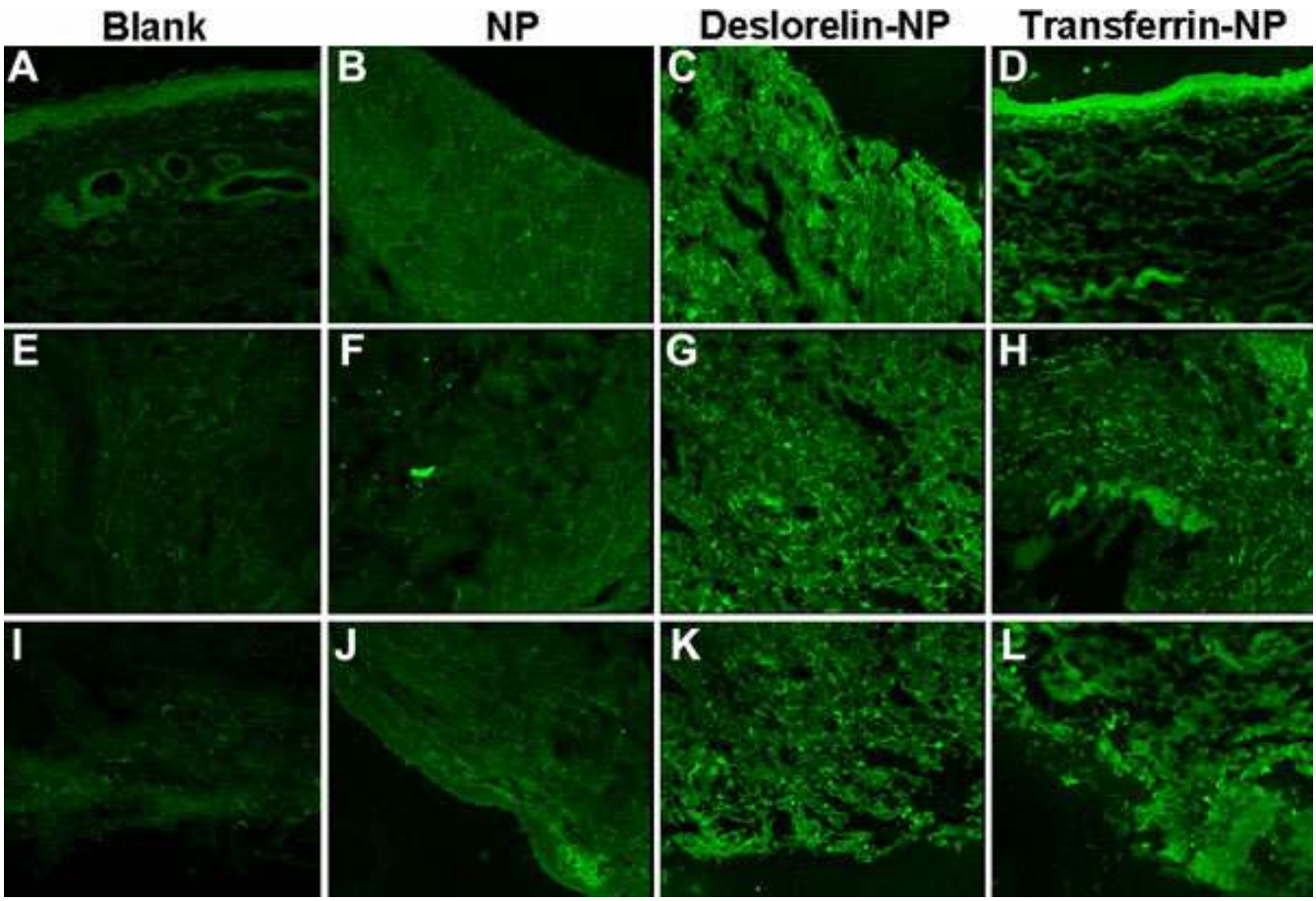

Figure 9. Representative confocal micrographs show the uptake of nanoparticles in the epithelial and stromal layers of bovine conjunctiva at the end of 4 h transport study at 37 °C using a modified Ussing chamber setup. **A**, **E**, and **I** represent the top, middle, and lower regions of blank conjunctival tissue without any nanoparticle exposure. Corresponding regions for NP (**B**, **F**, and **J**), deslorelin-NP (**C**, **G**, and **K**), and transferrin-NP (**D**, **H**, and **L**) are shown in various panels. Due to folding of conjunctiva, a clear distinction of epithelial and stromal layer could not be made in deslorelin-NP samples. The confocal images were obtained at a magnification of 20X.

ery [5]. Thus, a potential exists for the use of nanoparticles in enhancing the corneal uptake and in sustaining drug delivery. Such an approach would be useful for treating disorders of the anterior segment. If conjunctival uptake can also be enhanced, such an approach might be useful in facilitating noncorneal absorption of drugs into the anterior segment as well as the posterior segment. In the present study, using an ex vivo model, we determined that the uptake of even very small nanoparticles is modest in the corneal epithelium, and we further developed approaches to enhance the uptake and/or transport of these nanoparticles across cornea and conjunctiva.

In the in vivo situation, the precorneal residence of eye drops is very short and effective delivery to the cornea requires rapid binding and entry of drugs or carriers. Isolated tissue permeation experiments with cornea over a few hours, with continuous maintenances of source drug provides useful information regarding the permeability properties of the tissue. However, the in vivo situation can potentially be better simulated using an intact eye for an ex vivo model. Using such a model with the cornea facing upwards and the lower half of the eye maintained in a 37 °C bath, we administered a drop on the corneal surface and allowed it to freely drain, to simulate in vivo clearance. Then, we measured particle uptake at 5 and 60 min following thorough washing of the eye surface to remove any loosely adherent particles. The uptake is expected to be the highest for the solutes or carriers tightly bound to the corneal surface or for those that are rapidly taken up by the corneal epithelium. To maintain surface moisture and to simulate tear flow in part, we administered buffer drops (50 µl) every 15 min and sealed the water bath. This model is only an approximation of the in vivo situation and the flow dynamics and shear forces are more complex in vivo. However, this approach provides useful information, as discussed in this manuscript.

The ex vivo bovine eye model allowed the maintenance of corneal and corneal epithelial tight junctional architecture (Figure 2 and Figure 3). Further, it allowed the maintenance of barrier integrity, as indicated by lack of altered paracellular permeability (Figure 4) [19]. The maintenance of the barrier properties was further confirmed by the substantial elevation of nanoparticle uptake upon removal of the corneal epithelium (Figure 5). Further, neither the corneal endothelial weight nor the corneal stromal weight (after removal of epithelium) increased during the 60 min study (Table 2), suggesting that there was no significant swelling of the tissues during the duration of the study. The removal of corneal epithelium led to 45- and 32 fold higher levels of nanoparticles in the stroma at 5 and 60 min, respectively, compared to the levels in eyes with intact epithelium (Figure 5). The unmodified particle dose entering the entire cornea in the presence of epithelium at 5 min was 2.05% compared to 22.93% in the absence of corneal epithelium (Table 2). This indicates that corneal epithelium is the most significant barrier to topical nanoparticle delivery and hence, approaches to enhance epithelial uptake would benefit nanoparticle delivery.

Corneal epithelial uptake of nanoparticles can be potentially enhanced by engineering surface features suitable for rapid binding or uptake of nanoparticles by the corneal epithelium. These properties can be built into nanoparticles by coating them with ligands for cell surface receptors. Such receptor ligands, besides allowing a rapid interaction of nanoparticles with cell surface, will potentially allow cellular

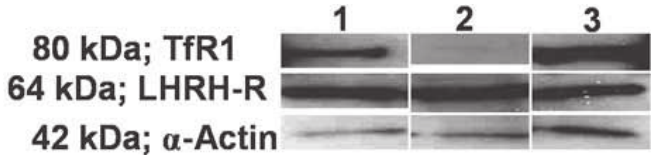

Figure 11. Differential expression of LHRH and transferrin receptors on various regions of bovine ocular tissue; western blot analysis. The panel shows LHRH-R, TfR-1, TfR-2 and α-actin bands as indicated. Lane 1 in the blot is pituitary, lane 2 represents corneal epithelium, and lane 3 is conjunctiva.

Table 3.

	Corneal epithelial uptake (%)		Corneal stromal uptake (%)	
Particle type	5 min	60 min	5 min	60 min
NP	1.05	1.90	1.32	1.58
Deslorelin-NP	3.38	8.54	5.54	3.82
Transferrin-NP	4.96	7.19	10.98	3.31

Nanoparticle uptake enhancement in the bovine ex vivo model upon surface functionalization with deslorelin and transferrin. The data are expressed as mean±SD for n=3.

Table 4.

	Corneal epithelial uptake (60 min; ng/mg tissue/mg dose)		
Particle type	Control (37 °C)	With free ligand (37 °C)	Control (4 °C)
Deslorelin-CA	1361.8±611.9	579.5±237.4*	463.3± 54.5*
Transferrin-CA	1146.3±306.6	467.1±131.9*	307.1±124*

Influence of free ligands and low temperature on the corneal epithelial uptake of deslorelin- and transferrin-functionalized nanoparticles in the bovine ex vivo model. Free ligands were used at a concentration of 1 mg/ml in the nanoparticle drop administered. The data are expressed as mean±SD for n=3. The asterisk indicates a $p<0.05$ compared to controls at 37 °C.

internalization of nanoparticles. We observed such benefits following modification of nanoparticle surface with deslorelin or transferrin.

In the present study, the uptake of deslorelin- and transferrin-conjugated nanoparticles was found to be higher as compared to plain nanoparticles in corneal epithelium (Figure 6 and Table 3). This uptake was sensitive to free ligand, with the extent decreasing in the presence of free deslorelin or transferrin (Table 4). This can be explained on the basis of receptor-mediated endocytosis of ligand functionalized nanoparticles and competition for the same by free ligands. Transferrin receptor has been shown to be expressed in human central as well as peripheral corneal epithelium [20]. Also, evidence exists for the ability of transferrin to enter cells via receptor-mediated endocytosis and subsequent transcytosis [21]. In this study, we also obtained real-time PCR evidence for corneal epithelial expression of transferrin (Figure 10). Further, a faint band for transferrin receptor 1 was observed using western blot analysis of corneal epithelium (Figure 11). We previously showed that deslorelin, an LHRH agonist, can be internalized and transcytosed across cell monolayers [22] and epithelial tissues [23]. Since there are no published reports on the expression of LHRH receptor in bovine ocular tissues, using western blot analysis and real-time PCR, we have for the first time ascertained that LHRH receptors are expressed on bovine corneal epithelium as well as conjunctiva (Figure 10 and Figure 11).

Upon conjugation with deslorelin and transferrin, nanoparticle uptake could be enhanced in the corneal epithelium by several fold. When unmodified nanoparticles were administered, the levels in tissue layers at 5 and 60 min were comparable, suggesting no additional advantage for binding or uptake with prolonged experimental times. In the 5 min experiment, the exposure ended at 5 min was followed by several washes to remove surface adherent particles. In the 60 min experiment, there were buffer drops administered every 15 min but this treatment may not have removed loosely adherent particles, which subsequently might have better adhered to corneal epithelium and entered the same. Possibly for this reason, with the deslorelin and transferrin conjugated particles, the tissue levels were greater at 60 min compared to 5 min.

A key observation of this study is the limited bioavailability of even 20 nm particles in the cornea epithelium, which was about 1.1-1.6% (Table 2 and Table 3). With the use of deslorelin and transferrin modifications, the corneal epithelial bioavailability could be increased to 3.4- and 5 fold, respectively. In the aqueous humor, no nanoparticles could be detected even at the end of 60 min, suggesting that the delivery of intact nanoparticles to aqueous humor is formidable even with the surface modifications used in this study. Noteworthy is the observation that even in the absence of corneal epithelium, nanoparticles were below detection limits in the aqueous humor at 60 min.

Stroma appears to be a good reservoir for nanoparticles, once they cross the corneal epithelium. By using LHRH agonist or transferrin as surface ligands, about 25 and 50% of stromal uptake achieved with epithelium removal is feasible, in the absence of any epithelial barrier perturbation. Even more remarkable is the observation that compared to an uptake of about 2.37% of plain nanoparticles into the cornea at the end of 5 min following eye drop administration (Table 3), LHRH agonist and transferrin functionalizations allow corneal delivery of about 9 and 16% of the dose within 5 min. This is a remarkable dose delivery, which is uniquely feasible with functionalized nanoparticles.

The above discussion pertained to the ex vivo model and carboxylate modified nanoparticles used in this study. The ex vivo model was devoid of full conjunctiva, and, therefore, we limited our analysis to the cornea and immediately underlying aqueous humor for particle quantification. However, from excised bovine eyes, a sheet of conjunctiva sufficient for permeability studies can be isolated. Therefore, in addition to the above ex vivo studies with eyeballs, using excised cornea and conjunctiva, we investigated the uptake and transport of nanoparticles with or without surface modifications. With isolated cornea and conjunctiva, we observed minimal transport of nanoparticles across the cornea as well as conjunctiva at the end of 4 h. Further, there was a significant lag time in the transport of nanoparticles, consistent with no uptake into aqueous humor in the ex vivo eyeball study. Excised tissue studies indicated that the conjunctiva is capable of slightly greater uptake and transport of nanoparticles compared to cornea (Figure 7). Greater permeability of nanoparticles across the conjunctiva compared to cornea is consistent with known differences in solute permeabilities across these two barriers [24]. Surface modification with deslorelin as well as transferrin increased the uptake of nanoparticles by both conjunctiva and cornea. Transport across cornea as well as conjunctiva was elevated by both surface modifications assessed. Further, low temperature reduced transport of all nanoparticle formulations across both tissues, suggesting energy-dependence of nanoparticle transport.

Unlike the cornea, for which epithelium, endothelium, and stroma are clearly distinguishable and easier to isolate, conjunctiva offers unique challenges. Trimming of the vasculature and other tissue mass beneath conjunctiva itself can alter conjunctival permeability [25]. We did not perform layer-by-layer analysis for conjunctiva since we have yet to establish methods for isolating conjunctival stroma samples in a reproducible manner. However, we performed confocal analysis of tissues isolated after in vitro transport studies. Confocal pictures of cornea and conjunctiva clearly show enhanced uptake of functionalized nanoparticles compared to plain nanoparticles (Figure 8 and Figure 9). Further, nanoparticle accumulation is localized clearly to the epithelium in the cornea. A similar primary localization is also evident in the conjunctival epithelium for transferrin-NP. For other particles in the conjunctiva, there was no such distinction, possibly due to the folding of tissue. However, it is noteworthy that there is more intense fluorescence distribution in the deeper regions (stroma) of conjunctiva compared to cornea.

Since nanoparticle systems have already been shown to persist in corneal and conjunctival tissues [26], with some of them providing greater drug levels in the intraocular tissues

[27], the surface modifications proposed in this study are expected to further enhance the corneal and conjunctival entry and hence the therapeutic value of nanoparticulate systems.

In summary, we have developed an ex vivo model to assess topical ocular delivery of solutes or drug carriers. The model maintained its integrity during the 60 min study. Our findings suggest the epithelium limited minimal uptake of 20 nm nanoparticles into the cornea and the potential of enhancing this uptake by modifying particle surface with an LHRH agonist or transferrin. These modifications can also enhance the uptake and transport of nanoparticles across the conjunctiva. Since the human eye surface is smaller, the percent uptake of nanoparticles will likely be lower and hence suitable approaches such as those proposed in this study are needed to engineer the particle surface for better cellular binding or entry. It is likely that such approaches will better enhance precorneal residence time, cellular uptake, and controlled release for nanoparticulate systems.

ACKNOWLEDGEMENTS

This work was supported by NIH grants DK064172 and EY013842. We thank Janice Taylor of the Confocal Laser Scanning Microscope Core Facility at the University of Nebraska Medical Center, which is supported by the Nebraska Research Initiative, for providing assistance with confocal microscopy. We thank Tom Bargar of Electron Microscopy facility for their assistance in obtaining nanoparticle images.

REFERENCES

1. Meadows DL, Paugh JR, Joshi A, Mordaunt J. A novel method to evaluate residence time in humans using a nonpenetrating fluorescent tracer. Invest Ophthalmol Vis Sci 2002; 43:1032-9.
2. Bourges JL, Gautier SE, Delie F, Bejjani RA, Jeanny JC, Gurny R, BenEzra D, Behar-Cohen FF. Ocular drug delivery targeting the retina and retinal pigment epithelium using polylactide nanoparticles. Invest Ophthalmol Vis Sci 2003; 44:3562-9.
3. Merodio M, Irache JM, Valamanesh F, Mirshahi M. Ocular disposition and tolerance of ganciclovir-loaded albumin nanoparticles after intravitreal injection in rats. Biomaterials 2002; 23:1587-94.
4. Marchal-Heussler L, Sirbat D, Hoffman M, Maincent P. Poly(epsilon-caprolactone) nanocapsules in carteolol ophthalmic delivery. Pharm Res 1993; 10:386-90.
5. Kompella UB, Bandi N, Ayalasomayajula SP. Subconjunctival nano- and microparticles sustain retinal delivery of budesonide, a corticosteroid capable of inhibiting VEGF expression. Invest Ophthalmol Vis Sci 2003; 44:1192-201.
6. Amrite AC, Ayalasomayajula SP, Cheruvu NP, Kompella UB. Single periocular injection of celecoxib-PLGA microparticles inhibits diabetes-induced elevations in retinal PGE2, VEGF, and vascular leakage. Invest Ophthalmol Vis Sci 2006; 47:1149-60.
7. Amrite AC, Kompella UB. Size-dependent disposition of nanoparticles and microparticles following subconjunctival administration. J Pharm Pharmacol 2005; 57:1555-63.
8. Giannavola C, Bucolo C, Maltese A, Paolino D, Vandelli MA, Puglisi G, Lee VH, Fresta M. Influence of preparation conditions on acyclovir-loaded poly-d,l-lactic acid nanospheres and effect of PEG coating on ocular drug bioavailability. Pharm Res 2003; 20:584-90.
9. Wood RW, Li VH, Kreuter J, Robinson JR. Ocular disposition of poly-hexyl-2-cyano[3-14C]acrylate nanoparticles in the albino rabbit. Int J Pharm 1985; 23:175-183.
10. de Campos AM, Diebold Y, Carvalho EL, Sanchez A, Alonso MJ. Chitosan nanoparticles as new ocular drug delivery systems: in vitro stability, in vivo fate, and cellular toxicity. Pharm Res 2004; 21:803-10. Erratum in: Pharm Res. 2005; 22:1007.
11. De Campos AM, Sanchez A, Alonso MJ. Chitosan nanoparticles: a new vehicle for the improvement of the delivery of drugs to the ocular surface. Application to cyclosporin A. Int J Pharm 2001; 224:159-68.
12. Aukunuru JV, Ayalasomayajula SP, Kompella UB. Nanoparticle formulation enhances the delivery and activity of a vascular endothelial growth factor antisense oligonucleotide in human retinal pigment epithelial cells. J Pharm Pharmacol 2003; 55:1199-206.
13. Aukunuru JV, Kompella UB. In vitro delivery of nano- and micro- particles to retinal pigment epithelial (RPE) cells. Drug Del Technol 2002; 2:50-57.
14. Bandi N, Kompella UB. Budesonide reduces multidrug resistance-associated protein 1 expression in an airway epithelial cell line (Calu-1). Eur J Pharmacol 2002; 437:9-17.
15. Roth C, Schricker M, Lakomek M, Strege A, Heiden I, Luft H, Munzel U, Wuttke W, Jarry H. Autoregulation of the gonadotropin-releasing hormone (GnRH) system during puberty: effects of antagonistic versus agonistic GnRH analogs in a female rat model. J Endocrinol 2001; 169:361-71.
16. Schirman-Hildesheim TD, Bar T, Ben-Aroya N, Koch Y. Differential gonadotropin-releasing hormone (GnRH) and GnRH receptor messenger ribonucleic acid expression patterns in different tissues of the female rat across the estrous cycle. Endocrinology 2005; 146:3401-8.
17. Halmos G, Schally AV, Kahan Z. Down-regulation and change in subcellular distribution of receptors for luteinizing hormone-releasing hormone in OV-1063 human epithelial ovarian cancers during therapy with LH-RH antagonist Cetrorelix. Int J Oncol 2000; 17:367-73.
18. Kawabata H, Yang R, Hirama T, Vuong PT, Kawano S, Gombart AF, Koeffler HP. Molecular cloning of transferrin receptor 2. A new member of the transferrin receptor-like family. J Biol Chem 1999; 274:20826-32.
19. Wang Y, Chen M, Wolosin JM. ZO-1 in corneal epithelium; stratal distribution and synthesis induction by outer cell removal. Exp Eye Res 1993; 57:283-92.
20. Lauweryns B, van den Oord JJ, Missotten L. The transitional zone between limbus and peripheral cornea. An immunohistochemical study. Invest Ophthalmol Vis Sci 1993; 34:1991-9.
21. Qian ZM, Li H, Sun H, Ho K. Targeted drug delivery via the transferrin receptor-mediated endocytosis pathway. Pharmacol Rev 2002; 54:561-87.
22. Koushik K, Bandi N, Sundaram S, Kompella UB. Evidence for LHRH-receptor expression in human airway epithelial (Calu-3) cells and its role in the transport of an LHRH agonist. Pharm Res 2004; 21:1034-46.
23. Koushik KN, Kompella UB. Transport of deslorelin, an LHRH agonist, is vectorial and exhibits regional variation in excised bovine nasal tissue. J Pharm Pharmacol 2004; 56:861-8.
24. Kompella UB, Sunkara G, Thomas E, Clark CR, Deruiter J. Rabbit corneal and conjunctival permeability of the novel aldose reductase inhibitors: N-[[4-(benzoylamino)phenyl] sulphonyl]glycines and N-benzoyl-N-phenylglycines. J Pharm Pharmacol 1999; 51:921-7.
25. Kompella UB, Kim KJ, Lee VH. Active chloride transport in the pigmented rabbit conjunctiva. Curr Eye Res 1993; 12:1041-8.

26. Zimmer A, Kreuter J, Robinson JR. Studies on the transport pathway of PBCA nanoparticles in ocular tissues. J Microencapsul 1991; 8:497-504.
27. Losa C, Calvo P, Castro E, Vila-Jato JL, Alonso MJ. Improvement of ocular penetration of amikacin sulphate by association to poly(butylcyanoacrylate) nanoparticles. J Pharm Pharmacol 1991; 43:548-52.

The print version of this article was created on 17 Oct 2006. This reflects all typographical corrections and errata to the article through that date. Details of any changes may be found in the online version of the article. α